Curvature Invariants for the Accelerating Natário Warp Drive

B. Mattingly[1,2]†, A. Kar[1,2], M. Gorban[1,2], W. Julius[1,2], C. Elmore[1,2], C. Watson[1,2], B. Shakerin[1,2], E. W. Davis[1,3] and G. B. Cleaver[1,2]

[1] *Early Universe, Cosmology and Strings* (EUCOS) *Group, Center for Astrophysics, Space Physics and Engineering Research* (CASPER), *Baylor University, Waco, TX 76798, USA*

[2] *Department of Physics, Baylor University, Waco, TX 76798, USA*

[3] *Institute for Advanced Studies at Austin, 11855 Research Blvd., Austin, TX 78759, USA*

Abstract: A process for using curvature invariants is applied to evaluate the accelerating Natário Warp Drive [1, 2]. Curvature invariants are independent of coordinate basis, and plotting the invariants is free of coordinate mapping distortions. While previous work focuses mainly on the mathematical description of the warp bubble, the method of plotting curvature invariants provides a novel pathway to investigate the Natário spacetime and its characteristics [3, 4].
The invariant plots demonstrate how each curvature invariant evolves over the variables of time, acceleration, skin depth and radius. They show that the Ricci Scalar has the greatest impact of the invariants on the surrounding spacetime. They also reveal key features of the Natário warp bubble such as a flat harbor in the center of it, a dynamic wake, and the internal structures of the warp bubble.

Keywords: Natário Warp Drive, Curvature Invariant, General Relativity.

PACS: 04.20.-q, 04.20.Cv, 02.40.-k.

1 Introduction

In Newtonian mechanics and special relativity, the velocity of any particle is fundamentally constrained by the speed of light, c. No particle can move through spacetime at a velocity greater than c in its reference frame. But, General relativity allows a global superluminal velocity. Alcubierre demonstrated a solution from the Einstien field equations

† mailto: *Brandon_Mattingly@Baylor.edu*

that allowed a spaceship to make a trip to a distant star in an arbitrarily short proper time [5]. He proposed a warping of spacetime that pairs a local contraction of spacetime in front of the spaceship with a local expansion of spacetime behind the ship. While the spaceship remains within its own light cone and never exceeds c, globally the relative velocity* may be much greater than c. He named the faster-than-light (FTL) propulsion mechanism based on this principle a "warp drive."

FTL travel obeys eight general requirements [6]. First, the rocket equation is not required for travel by way of the warp. Second, the travel time through the FTL space warp to a distant star should take less than one year as seen both by the passengers in the warp and by stationary observers outside the warp. Third, the proper time as measured by the passengers will not be dilated by any relativistic effects. Fourth, it is possible to minimize any tidal-gravity accelerations acting on any passengers less than the acceleration of gravity near the Earth's surface, $g_{\oplus}$. Fifth, the local speed of any passengers should be less than c. Sixth, the matter of the passengers must not couple with any exotic material needed to generate the FTL space warp. Seventh, the FTL space warp should not generate an event horizon. Finally, the passengers should not encounter a singularity inside or outside of the FTL warp.

Traversable wormholes and warp drives are two known examples that satisfy these eight requirements [1, 5, 7, 8, 9, 10, 11, 12]. While they are mathematical solutions to Einstein's equations, building such devices are not achievable in the foreseeable future due to severe engineering constraints. In [4], the authors used the method of calculating and plotting curvature invariants to analyze several types of wormholes. In the present work, the authors will adapt this methodology to analyze the accelerating Natário Warp Drive.

Since Alcubierre, there has been considerable research into FTL warp drives. In [7], Krasnikov considered a non-tachyonic FTL warp bubble and showed it to be possible mathematically. Van Den Broeck in [8] modified Alcubierre's warp drive to have a microscopic surface area and a macroscopic volume inside. He showed that the modification allowed a warp bubble with more reasonable energy requirements of a few solar masses to form the warp bubble and the geometry has more lenient violation of the null-energy-conditions (NEC). Later, Natário improved upon Alcubierre's work by presenting a warp drive metric such that zero spacetime expansion occurs [1]. Instead of riding a contraction and expansion of spacetime, the warp drive may be observed to be "sliding" through the exterior spacetime at a constant global velocity. Finally in [2], Loup expanded Natário's work to encompass an accelerating global velocity.

While the mathematics of a warp drive is well developed, mapping the spacetime around the warp drive remains unexplored until recently. Considering that a ship inside of a warp bubble is causally disconnected from the exterior [1], computer simulations of the surrounding spacetime are critical for the ship to map its journey and steer the warp bubble. In [5], Alcubierre uses the York time† to map the volume expansion of a warp drive. He plotted

*defined as proper spatial distance divided by proper time

†The York time is defined as $\Theta = \frac{v_s}{c}\frac{x-x_s}{r_s}\frac{df}{dr_s}$

the York time to show how spacetime warped behind and in front of the spaceship. While the York time is appropriate when the 3-geometry of the hypersurfaces is flat, it will not contain all information about the curvature of spacetime in non-flat 3-geometries such as the accelerating Natátio warp drive spacetime. The best way to properly illustrate general warp drive spacetimes is to derive and plot their independent curvature invariants.

Christoffel proved that scalars constructed from the metric and its derivatives must be functions of the metric itself, the Riemann tensor, and its covariant derivatives [13]. Curvature invariants are scalar products of Riemann, Ricci or Weyl tensors, or their covariant derivatives. To visualize curved spacetime phenomena without distortion is to plot only the curvature invariants – quantities whose value are the same regardless of the choice of coordinates. Fourteen curvature invariants in $3+1D$ have been defined in the literature, but the total rises to seventeen when certain non-degenerate cases are taken into account [14]. Carminati and McLenaghan (CM) demonstrated a set of invariants that had several attractive properties. Their invariant set maintains general independence, requires each invariant to be of lowest possible degree, and contains a minimal independent set for any Petrov type and choice of Ricci Tensor [15]. For the case of Class B spacetimes, the syzgies between the invariants further reduces the independent set of invariants to be only the four specific ones: R, r_1, r_2 and w_2 [16].

Henry et al. [3] conducted a study which computed and plotted a number of independent curvature invariants for the hidden interiors of Kerr-Newman black holes. They produced visually stunning 3D plots which revealed the surprisingly complex nature of spacetime curvature in Kerr-Newman black hole interiors. The calculation of curvature invariants in Black Holes is a rich topic of recent study [17, 18, 19, 20, 21]. This work motivated the present authors to undertake a similar study for Natário Warp Drive.

2 Method to Compute the Invariants

The CM curvature invariants can be calculated from any given line element. From the line element, the metric g_{ij} is identified with the indices $\{i, j, k, l\}$ ranging from $\{0, n-1\}$, where n is the number of spacetime dimensions. The accelerating Natário Warp Drive was derived using $n = 4$ [2]. In spacetime, a complex null tetrad may be identified from a given line element. In this paper, a null tetrad $(l_i, k_i, m_i, \bar{m}_i)$ is found for the accelerating Natário metric. It is emphasized that the scalar invariants are independent of the choice of coordinates in the null tetrad. A different choice of coordinates for each spacetime's tetrad will result in the same invariants plotted in this paper. From the metric, the affine connection $\Gamma^i{}_{jk}$, Riemann tensor $R^i{}_{jkl}$, Ricci tensor R_{ij}, Ricci scalar R, trace free Ricci tensor S_{ij} and Weyl tensor C_{ijkl} is calculated. The Newman-Penrose (NP) curvature components may be computed from the null tetrad, the Ricci Tensor, and the Weyl Tensor [22]. The thirteen different CM invariants are defined in [15]. Only four of these invariants are required by the syzgies for Class B spacetimes: the Ricci Scalar, the first two Ricci invariants, and the real component of the Weyl Invariant J [16]. In terms of the NP curvature coordinates, the CM

invariants are:

$$R = g_{ij}R^{ij}, \tag{1}$$

$$\begin{aligned} r_1 &= \frac{1}{4}S_a{}^b S_b{}^a \\ &= 2\Phi_{20}\Phi_{02} + 2\Phi_{22}\Phi_{00} - 4\Phi_{12}\Phi_{10} - 4\Phi_{21}\Phi_{01} + 4{\Phi_{11}}^2, \end{aligned} \tag{2}$$

$$\begin{aligned} r_2 &= -\frac{1}{8}S_a{}^b S_c{}^a S_b{}^c \\ &= 6\Phi_{02}\Phi_{21}\Phi_{10} - 6\Phi_{11}\Phi_{02}\Phi_{20} + 6\Phi_{01}\Phi_{12}\Phi_{20} - 6\Phi_{12}\Phi_{00}\Phi_{21} - 6\Phi_{22}\Phi_{01}\Phi_{10} + 6\Phi_{22}\Phi_{11}\Phi_{00}, \end{aligned} \tag{3}$$

$$w_2 = -\frac{1}{8}\bar{C}_{abcd}\bar{C}^{abef}\bar{C}^{cd}{}_{ef} = 6\Psi_4\Psi_0\Psi_2 - 6{\Psi_2}^3 - 6{\Psi_1}^2\Psi_4 - 6{\Psi_3}^2\Psi_0 + 12\Psi_2\Psi_1\Psi_3. \tag{4}$$

3 Warp Drive Spacetimes

Alcubierre and Natário developed warp drive theory using 3+1 ADM formalism. Spacetime is decomposed into space-like hypersurfaces parametrized by the value of an arbitrary time coordinate dx^0 [23, 24]. Two nearby hypersurfaces, x^0 = constant and $x + dx^0$ = constant, are separated by a proper time $d\tau = N(x^\alpha, x^0)dx^0$. The ADM four-metric is

$$g_{ij} = \begin{pmatrix} -N^2 - N_\alpha N_\beta g^{\alpha\beta} & N_\beta \\ N_\alpha & g_{\alpha\beta} \end{pmatrix}, \tag{5}$$

where N is the lapse function and N_α is the shift vector between hypersurfaces. A warp drive is defined as a globally hyperbolic spacetime (M, g), where $M = \mathbb{R}^4$ and g is given by the line element

$$ds^2 = -dt^2 + \sum_{i=1}{}^3 (dx^i - X^i dt)^2, \tag{6}$$

for three unspecified bounded smooth functions $(X^i) = (X, Y, Z)$ in Cartesian coordinates [1, 5]. The functions form a vector field given by $\mathbf{X} = X^i \frac{\partial}{\partial x^i} = X\frac{\partial}{\partial x} + Y\frac{\partial}{\partial y} + Z\frac{\partial}{\partial z}$. $\mathbf{X}$ is a time-dependant vector field in Euclidean 3-space. Six line elements for the Natário spacetime metric with constant acceleration have been derived [2]. The specific equation for the Natário warp drive line element in the parallel covariant 3 + 1 ADM is

$$ds^2 = \big(1 - 2X_t + (X_t)^2 - (X_{r_s})^2 - (X_\theta)^2\big)dt^2 + 2\big(X_{r_s}dr_s + X_\theta r_s d\theta\big)dt - {dr_s}^2 - {r_s}^2 d\theta^2 - {r_s}^2 \sin^2\theta d\phi^2. \tag{7}$$

which is in the spherical coordinates[‡] and a is the constant acceleration. The covariant shift vector components are given by

$$X_t = 2n(r_s)ar_s\cos\theta, \tag{8}$$

$$X_{r_s} = 2[2n(r_s)^2 + r_s n'(r_s)]at\cos\theta, \tag{9}$$

$$X_\theta = -2n(r_s)at[2n(r_s) + r_s n'(r_s)]{r_s}^2\sin\theta. \tag{10}$$

The Natário warp drive continuous shape function is

$$n(r_s) = \frac{1}{2}\left[1 - \frac{1}{2}\Big(1 - \tanh[\sigma(r_s - \rho)]\Big)\right]. \tag{11}$$

[‡] $(0 \leqslant r_s < \infty;\ 0 \leqslant \theta \leqslant \pi;\ 0 \leqslant \varphi \leqslant 2\pi)$, and $(-\infty < t < \infty)$

where σ is the skin depth of the warp bubble and ρ is the radius of the warp bubble. Appendix A.2 derives the comoving null tetrad for Equation (7). It is

$$l_i = \begin{pmatrix} 1 - X_t + X_{r_s} \\ -1 \\ 0 \\ 0 \end{pmatrix}, \qquad k_i = \begin{pmatrix} 1 - X_t - X_{r_s} \\ 1 \\ 0 \\ 0 \end{pmatrix},$$
$$m_i = \begin{pmatrix} X_\theta \\ 0 \\ -r \\ ir\sin\theta \end{pmatrix}, \qquad \bar{m}_i = \begin{pmatrix} X_\theta \\ 0 \\ -r \\ -ir\sin\theta \end{pmatrix}. \tag{12}$$

The comoving null tetrad describes light rays traveling parallel with the warp bubble. The four CM invariants in Equations (1) through (4) may be derived from Equations (7) and (12).

4 Invariants for the Accelerating Natário Warp Drive

The computations and plots for the four CM invariants in Equations (1), (2), (3), and (4) from the accelerating Natário Warp drive are found by Mathematica® and presented herein. The free variables in the accelerating Natário warp drive are a, ρ, σ, and t in Equations (8) through (11). To see the effect of the free variables on the surrounding curvature invariants, each one was varied individually while maintaining all other variables constant. Through this procedure, 684 plots were rendered for each invariant and are provided in the supplementary files. For the remainder of the paper, a sample of these plots will be shared and inspected to see the effect of each variable on the curvature invariants.

4.1 Invariant Plots while Varying the Time

The invariants evolve dynamically over time. Figure 1 in Appendix A.2 shows how the Ricci Scalar evolves from $t = 0\ s$ to $t = 100\ s$, while setting $\rho = 100\ m$, $\sigma = 50000\ m^{-1}$, and $a = 1.0\ ms^{-2}$. The figures provide rich details of the features in and around the warp bubble. Each plot has a safe harbor within $\rho \leqslant 100\ m$ where the curvature plots are flat. A spaceship riding in the interior of the harbor would experience only flat space throughout the entire time evolution. The warp bubble travels perpendicular to the wake along the $\theta = (\frac{\pi}{2}, \frac{3\pi}{2})$ line. The wake is a volume of large curvature as shown on the plots. While the form of the wake quickly reaches a constant shape, the Ricci scalar's magnitude increases approximately proportional to time. The linear increase in the warp bubble's curvature suggests an engineering constraint on a maximum achievable global velocity. The wake's shape also shows that there is internal structure to the warp bubble. Finally, it can be seen that far in front and behind the warp bubble that the invariants are zero; thus, the space is asympotically flat.

Choosing the same values for ρ, σ, and a as the Ricci Scalar and varying the time, Figure 2 in Appendix A.2 shows the time evolution for the r_1 invariant. It has many similar features to the Ricci Scalar. It contains the safe harbor, a wake running perpendicular to

the direction of motion, is asymptotically flat in front and behind the bubble, and increases approximately linearly with time. The first apparent difference is the positive magnitude and lack of internal structure in the wakes. The wake increases subtly in angular size as time increases.

The invariant r_2 shares the same basic properties of the Ricci Scalar and r_1: the safe harbor, a wake, is asymptotically flat away from the bubble, and a linear increase with time. It is similar in shape to r_1, but it increases in magnitude more drastically and has the same internal structure as the Ricci Scalar.

The invariant w_2 shares the same basic properties of the Ricci Scalar, r_1, and r_2: the safe harbor, a wake, is asymptotically flat away from the bubble, and a linear increase with time. The invariant's wake contains a small amount of internal structure at lower time values, but as time reaches 100 s, the internal structures begins to form crenulations. As time continues to evolve, the crenulations travel out parallel to the length of the wake from the center of warp bubble. It can be speculated that this would cause an erratic flight path of the bubble since the crenulations are not symmetric. It can also be speculated that the Ricci Scalar and r_2 would exhibit additional behavior at higher time values.

4.2 Invariant Plots while Varying the Acceleration

Varying the acceleration of the invariants speeds up or slows down the time evolution in the previous section. Setting $\rho = 100\ m$, $\sigma = 50000\ m^{-1}$, and $t = 1.0\ s$, Figure 5 in Appendix A.2 shows the acceleration's variation for the Ricci Scalar. The first plot of $a = 0\ ms^{-2}$ is consistent with the lapse function being zero for all time. The distance between hypersurfaces will be constant. The space will be flat and no warp bubble will form as is shown. The second plot corresponds to a time slice between Figures 1a and 1b. Similarly, the third plot is identical to Figure 1c, and the fourth plot corresponds to a time slice after Figure 1d. It can be concluded that modifying the acceleration parameter corresponds with modifying the rate of change of the hypersurfaces. Additionally, our analysis in the previous section holds.

The plots of the invariants r_1 and r_2 follow a similar process as the Ricci Scalar. They are plotted in Figure 5 in Appendix A.2. When $a = 0$, their plots are identical to Figure 5a. Then, they can be seen as additional time slices between the plots shown in Figures 2a and 2b for r_1 and 3c and 3d for r_2. Some additional features are present in the plots. The invariants do warp themselves much more significantly and non-symmetricly than their counterparts for the Ricci Scalar as can be seen in Figure 7c.

4.3 Invariant Plots while Varying the Skin Depth of the Warp Bubble

Varying the skin depth of the warp bubble, σ, does not noticeably affect the invariant plots. Figure 9 in Appendix A.2 presents the plots for each of the four invariants while doubling the skin depth and setting $\rho = 100000\ m^{-1}$, $t = 1.0$ s, and $a = 1.0\ ms^{-2}$. The shape of the invariant does not change in the figures after the doubling. It can be speculated that either the invariants are independent of skin depth or that the impact of skin depth is minimal compare to the other variables.

4.4 Invariant Plots while Varying the Radius of the Warp Bubble

Varying the radius of the warp bubble, ρ, increases the size of the safe harbor inside the invariants. Setting $\rho = 100\ m$, $t = 1.0\ s$, and $a = 1.0\ ms^{-2}$, the following plots for the invariants result in Figure 6 in Appendix A.2. In the figure, the radial coordinate clearly doubles in each invariant without affecting the shape of the plots. The safe harbor of $\rho \leqslant 100\ m$ in the left hand column also doubles in size to $\rho \leqslant 200\ m$. The only other pertinent feature is in the internal structure of w_2. The structures are reduced implying that they cluster near the center.

5 Conclusion

This paper demonstrates how computing and plotting the curvature invariants for various variables of warp drive spacetimes can reveal their underlying features. While the individual functions are mammoth in size and take a long time to calculate, their plots can be quickly scanned and understood. The plots give the magnitude of curvature at each point around the ship. Where the plots' magnitudes are large, space is greatly warped and vice versa. Also observing the changes in slopes on the plots, the rate at which spacetime is being folded can be approximated. This information can be used to map the spacetime around the ship and aid potential navigation.

In this paper, the accelerating Natário warp drive metric was plotted for different choices of the variables t, a, ρ, σ. In all plots of the listed variables, the constant features include a safe harbor, a wake running perpendicular to the warp bubble's direction of motion, and an asympotically flat space far away from the bubble. By varying time, each invariant's plots experience a sudden jump from positive curvature in the direction of motion to negative curvature. As time progresses, the shape of the R, r_1, and r_2 invariants remains constant, but the magnitude of the invariants increases somewhat linearly and the angular arc widens slightly. The invariant w_2 begins to exhibit crenulations in the interior of the warp bubble after 100 s. By varying the acceleration, the invariant plots skip through the time slices. Internal structures become more prominent. Changing the skin depth did not change either

the shape or magnitude of the invariant plots. Doubling the radius did double the size of the safe harbor without affecting the plots in any other way. The invariant plots give a rich and detailed understanding of the warp bubble's curvature.

Computing and plotting the invariant functions has significant advantages for the inspection of warp drives and their potential navigation. As mentioned previously, plotting the invariants has the advantage that they are free from coordinate mapping distortions, divergences, discontinuities or other artifacts of the chosen coordinates. Once the invariant plots reveal the location of any artifacts, their position can be related mathematically to the standard tensors, and their effect on an objects motion can then be analyzed. The invariant plots properly illustrate the entire underlying spacetime independent of a chosen coordinate system. A second advantage is the relative ease with which the invariants can be plotted. Software packages exist or can be developed to calculate the standard tensors. The aforementioned tensors lead to a chosen basis of invariants. While the CM invariants were chosen in this paper, other sets of invariants exist such as the Cartan invariants and the Witten and Petrov invariants [21, 25]. It is an open problem to inspect the curvature of the warp drive spacetimes in these invariant sets. It is expected that the main features identified in this paper will also hold in these different bases.

In addition to inspecting different invariant bases, further work can be done in mapping warp drive spacetimes. The work in this paper can be further expanded on greater time slices. Potentially, crenulations like the ones observed for w_2 exist within the warp bubbles for R, r_1 and r_2. It can be speculated that the crenulations and the linear increase in the magnitude of the curvature establishes a linear increase in the amount of energy required to accelerate the warp bubble to arbitrarily high velocities. This relation implies that engineering an arbitrarily fast warp drive is challenging. The longer the warp drive accelerates and/or the greater the magnitude of acceleration results in a greater magnitude of curvature and requires a larger amount of energy. This relationship suggests that a realistic warp drive would only be able to accelerate to some finite velocity potentially greater than c. This could be the evidence for a less restrictive superluminal censorship theorem than previously considered in [26]. Further research is needed to establish the maximum achievable velocity for a warp drive. In addition, the crenulations imply that high frequency gravitational waves would be produced by an accelerating warp drive. Potentially, these waves could be detected by an extremely sensitive detector. A detector like the one proposed by [27] would be suitable. Finally, the technique of plotting the invariants can be applied to other warp drive spacetimes such as Alcubierre, Krasnikov, Van Den Broek or Natário's at a constant velocity.

6 Acknowledgements

E. W. Davis would like to thank the Institute for Advanced Studies at Austin for supporting this work. B. Mattingly would like to thank D. D. McNutt for beneficial discussions.

A Appendices

A.1 Null Vectors of the Natário Metric

A null tetrad contains two real null vectors, $\mathbf{k}$ and $\mathbf{l}$, and two complex conjugate null vectors, $\mathbf{m}$ and $\bar{\mathbf{m}}$ that satisfy the following algebraic relationships [22]:

$$\mathbf{e_a} = (\mathbf{m}, \bar{\mathbf{m}}, \mathbf{l}, \mathbf{k}), \tag{12}$$

$$g_{ab} = 2m_{(a}\bar{m}_{b)} - 2k_{(a}l_{b)} = \begin{pmatrix} 0 & 1 & 0 & 0 \\ 1 & 0 & 0 & 0 \\ 0 & 0 & 0 & -1 \\ 0 & 0 & -1 & 0 \end{pmatrix}. \tag{13}$$

Given an orthonormal tetrad, $\mathbf{E_a}$, it can be related to a complex null tetrad Equation (12) by:

$$\begin{aligned} l_i &= \frac{1}{\sqrt{2}}(E_1 + E_2), & k_i &= \frac{1}{\sqrt{2}}(E_1 - E_2), \\ m_i &= \frac{1}{\sqrt{2}}(E_1 + iE_2), & \bar{m}_i &= \frac{1}{\sqrt{2}}(E_1 - iE_2). \end{aligned} \tag{14}$$

The line element in Equation (7) has an orthonormal tetrad:

$$\begin{aligned} E_1 &= \begin{pmatrix} 1 - X_t & 0 & 0 & 0 \end{pmatrix}, & E_2 &= \begin{pmatrix} X_{r_s} & -1 & 0 & 0 \end{pmatrix}, \\ E_3 &= \begin{pmatrix} X_\theta & 0 & -r & 0 \end{pmatrix}, & E_4 &= \begin{pmatrix} 0 & 0 & 0 & r\sin\theta \end{pmatrix}. \end{aligned} \tag{15}$$

Using Mathematica®, it can be verified that

$$g_{ij} = E_i \cdot E_j. \tag{16}$$

and by applying the equations Equations (14) to (15) the null vectors in Equation (12) result.

A.2 Invariant Plots

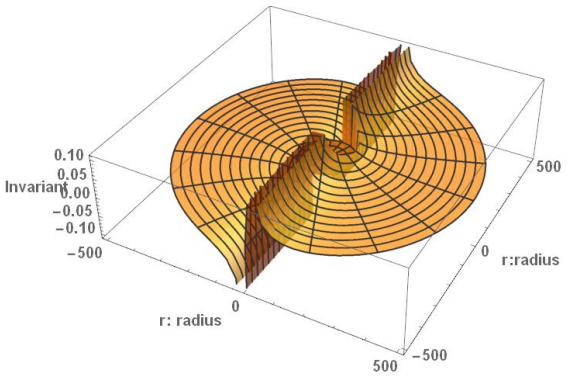

(a) $t = 0.0s$

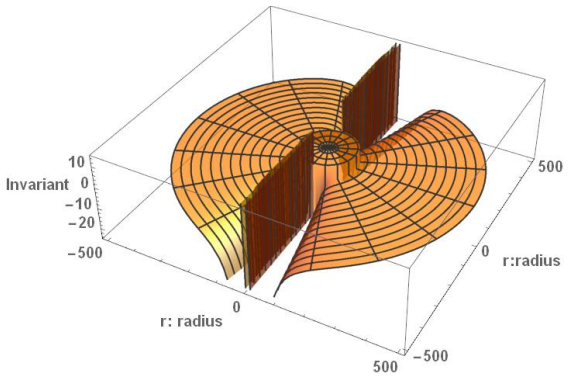

(b) $t = 1.0s$

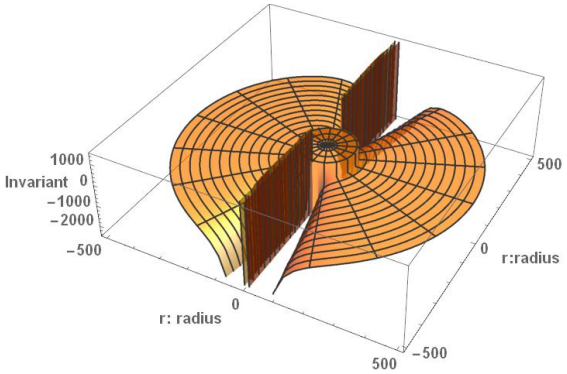

(c) $t = 10.0s$

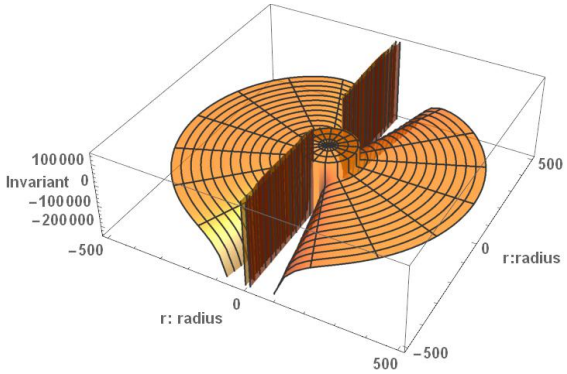

(d) $t = 100.0s$

Figure 1: Time evolution of R, the Ricci Scalar

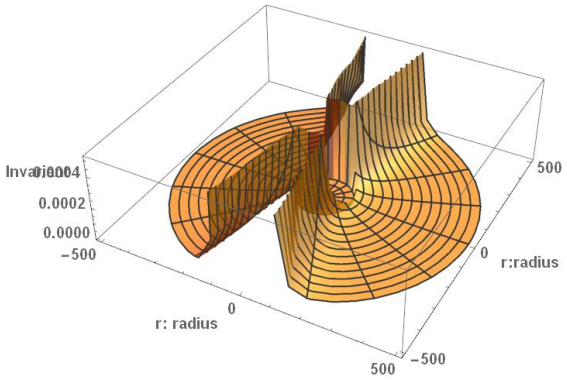

(a) r_1 and $t = 0.0s$

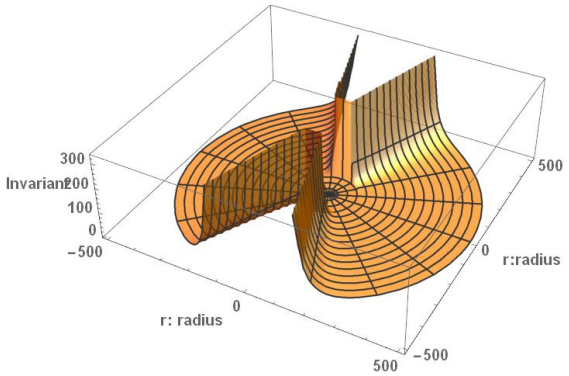

(b) r_1 and $t = 1s$

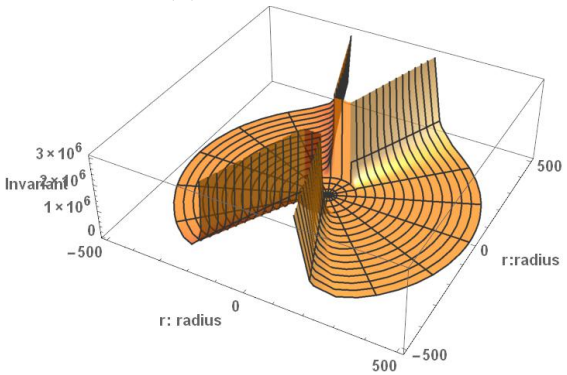

(c) r_1 and $t = 10s$

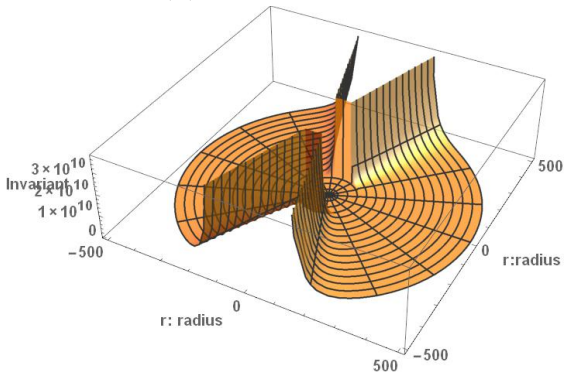

(d) r_1 and $t = 100s$

Figure 2: Time evolution of the invariant r_1

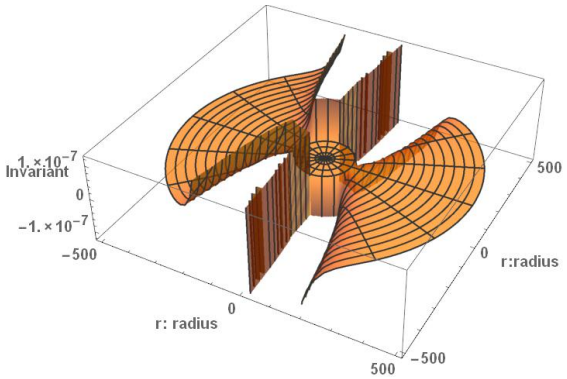

(a) r_2 and $t = 0.0s$

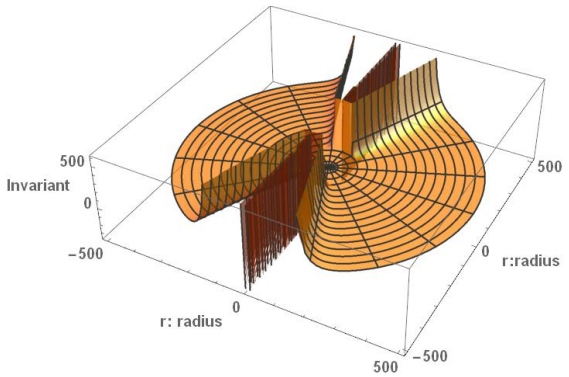

(b) r_2 and $t = 1s$

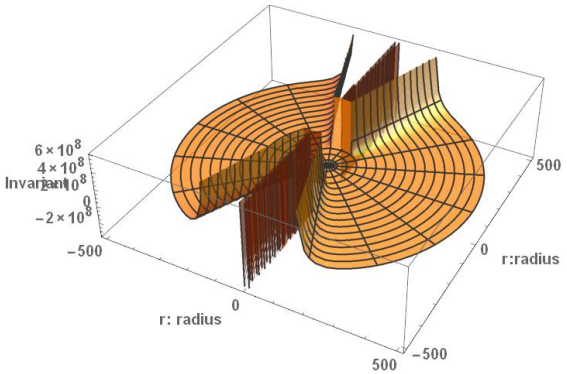

(c) r_2 and $t = 10s$

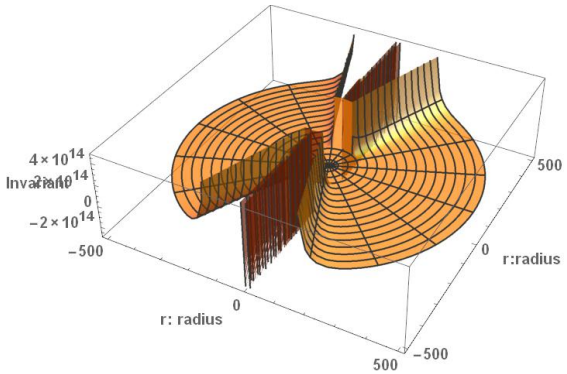

(d) r_2 and $t = 100s$

Figure 3: Time evolution of the invariant r_2

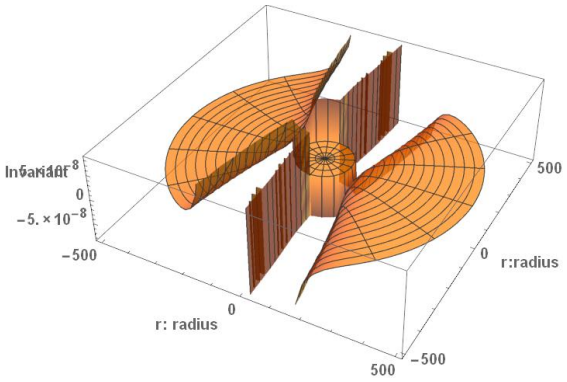

(a) w_2 and $t = 0s$

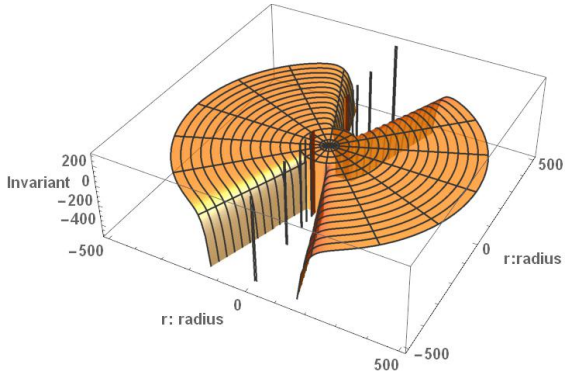

(b) w_2 and $t = 1.0s$

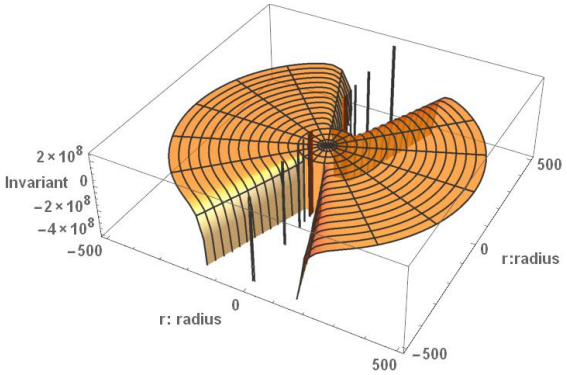

(c) w_2 and $t = 10.0s$

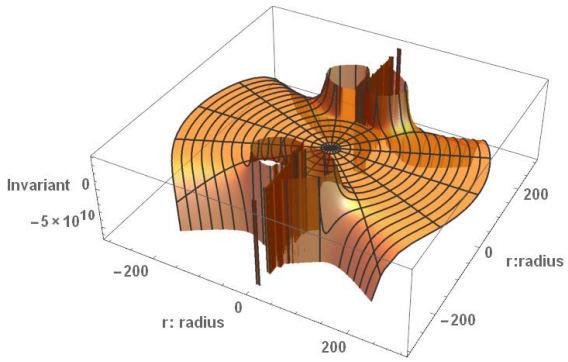

(d) w_2 and $t = 100.0s$

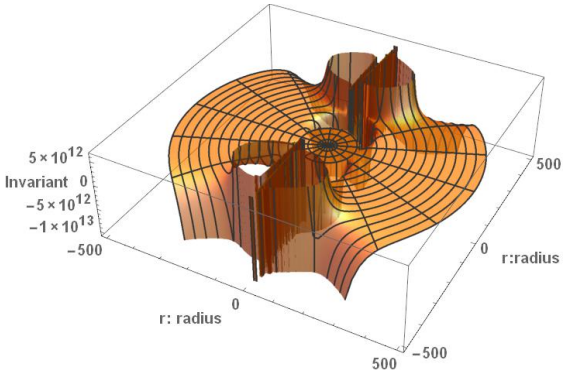

(e) w_2 and $t = 200.0s$

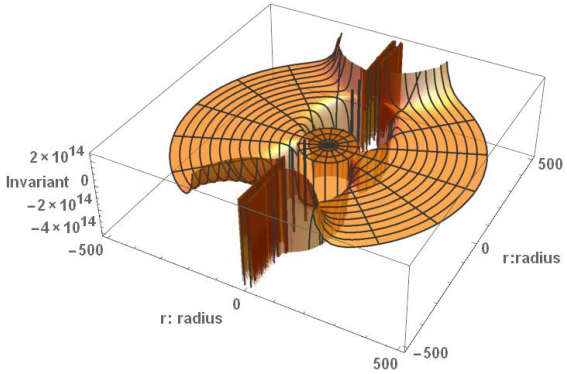

(f) w_2 and $t = 300.0s$

Figure 4: Time evolution of the Invariant w_2

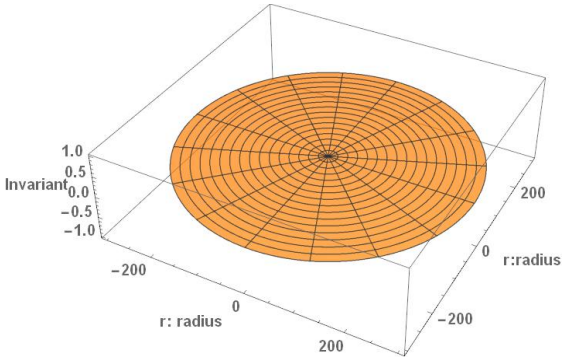

(a) $a = 0.0ms^{-2}$

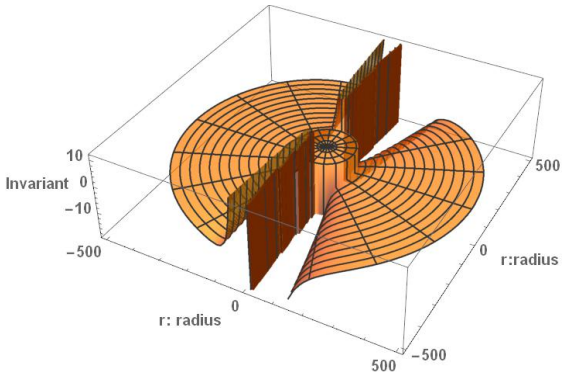

(b) $a = 0.11ms^{-2}$

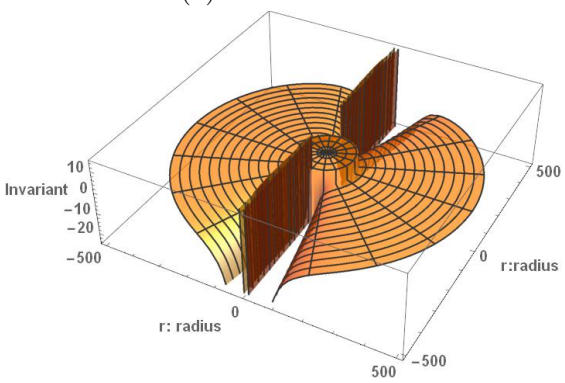

(c) $a = 1.0ms^{-2}$

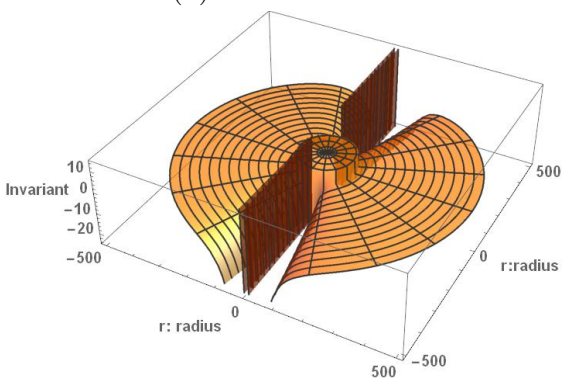

(d) $t = 10.0ms^{-2}$

Figure 5: Acceleration evolution of R, the Ricci Scalar

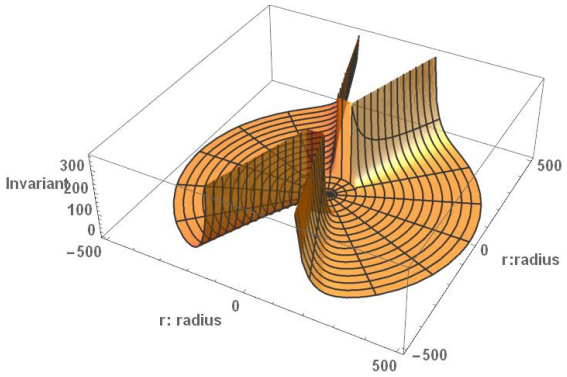

(a) r_1 and $a = 0.1ms^{-2}$

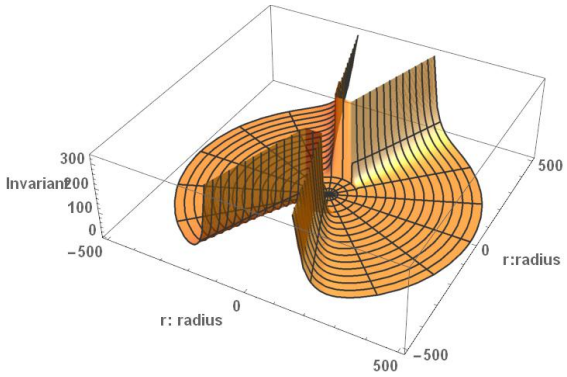

(b) r_1 and $a = 1.0ms^{-2}$

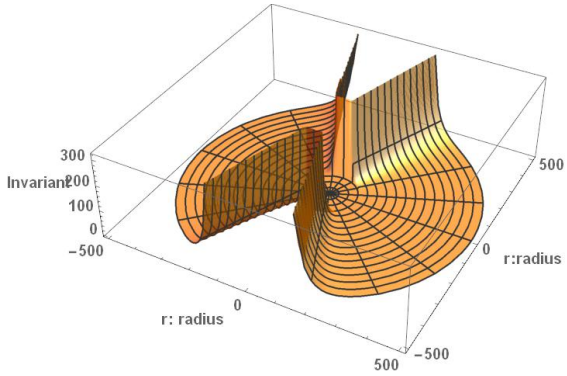

(c) r_1 and $a = 10.0ms^{-2}$

Figure 6: Acceleration evolution of the Invariant r_1

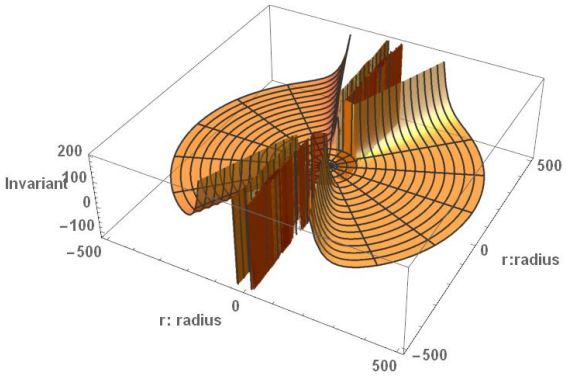

(a) r_2 and $a = 0.1ms^{-2}$

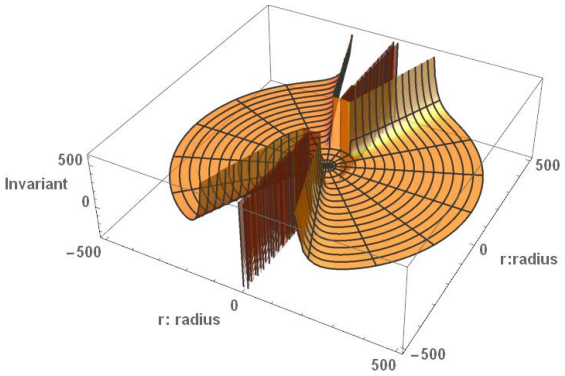

(b) r_2 and $a = 1.0ms^{-2}$

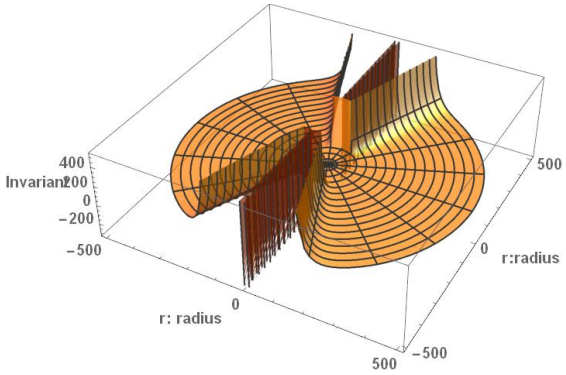

(c) r_2 and $a = 10.0ms^{-2}$

Figure 7: Acceleration evolution of the Invariant r_2

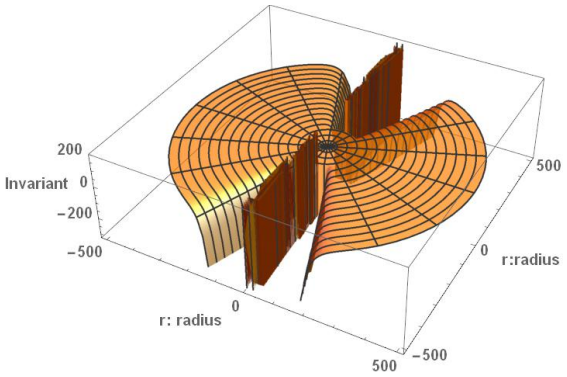

(a) w_2 and $a = 0.1ms^{-2}$

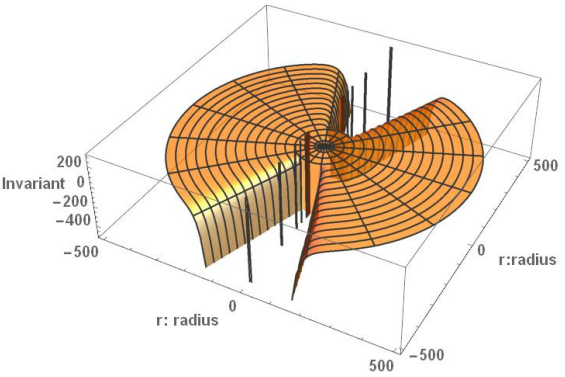

(b) w_2 and $a = 1.0ms^{-2}$

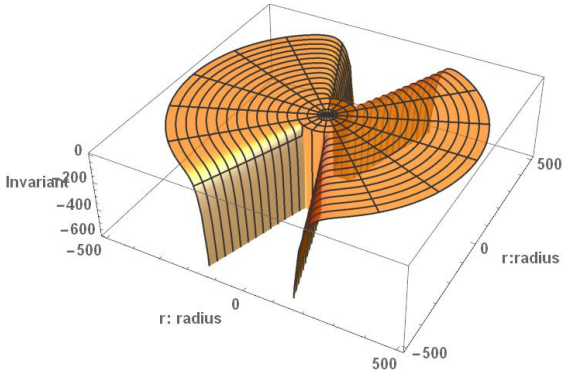

(c) w_2 and $a = 10.0ms^{-2}$

Figure 8: Acceleration evolution of the Invariant w_2

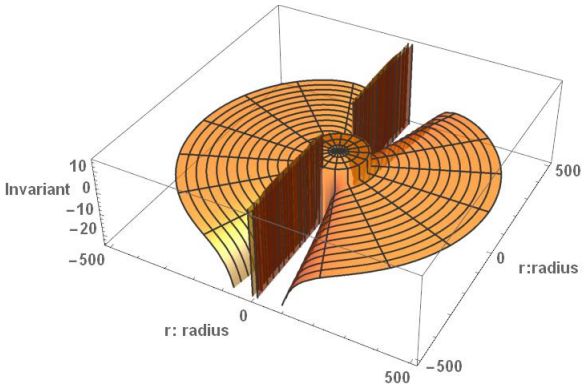

(a) Ricci Scalar with $\rho = 100m$

(b) Ricci Scalar with $\rho = 200m$

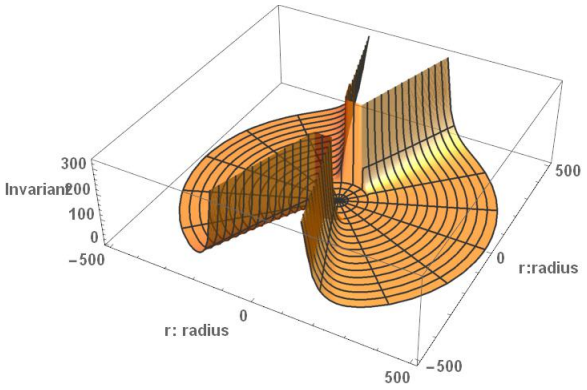

(c) The invariant r_1 with $\rho = 100m$

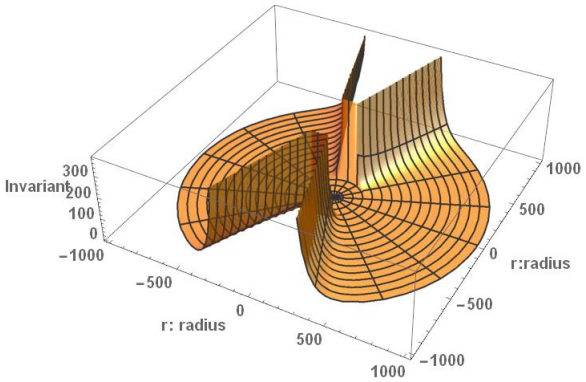

(d) The invariant r_1 with $\rho = 200m$

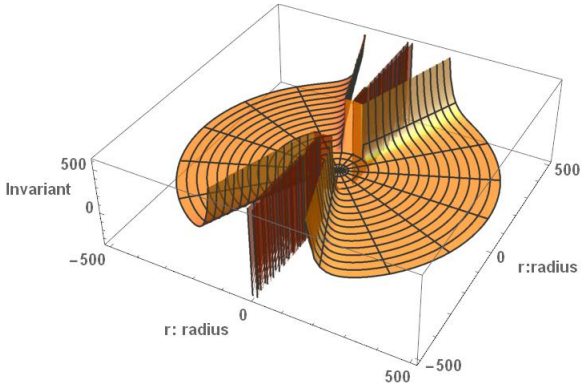

(e) The invariant r_2 with $\rho = 100m$

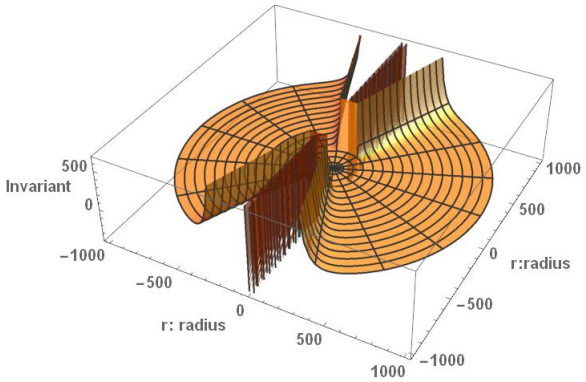

(f) The invariant r_2 with $\rho = 200m$

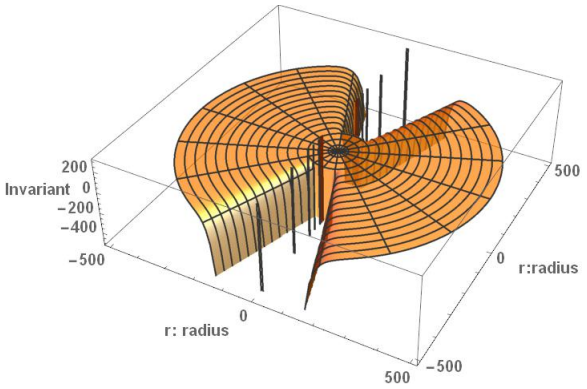

(g) The invariant w_2 with $\rho = 100m$

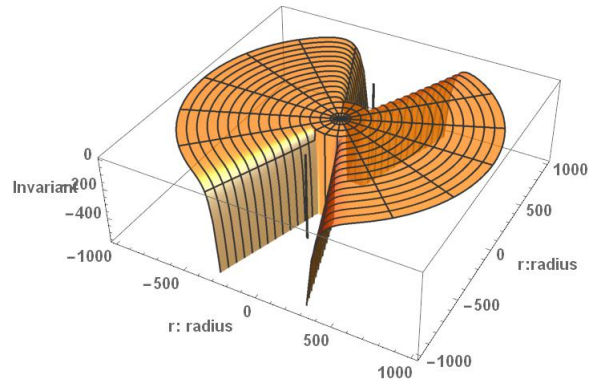

(h) The invariant w_2 with $\rho = 200m$

Figure 9: The warp bubble radius of the R, r_1, r_2, and w_2

References

[1] J. Natário, "Warp drive with zero expansion", Class. Quant. Grav. **19**, 1157 (2002) doi:10.1088/0264-9381/19/6/308 [gr-qc/0110086].

[2] Fernando Loup. An extended version of the Natário warp drive equation based in the original 3 + 1 ADM formalism which encompasses accelerations and variable velocities. [Research Report] Residencia de Estudantes Universitas. 2017. $< hal - 01655423 >$

[3] J. Overduin, M. Coplan, K. Wilcomb and R. C. Henry, "Curvature Invariants for Charged and RotatingBlack Holes," Universe **6**, no.2, 22 (2020) doi:10.3390/universe6020022

[4] Mattingly, B. et al. (2018), "Curvature Invariants for Lorentzian Traversable Wormholes", arXiv:1806.10985v1 [gr-qc].

[5] M. Alcubierre, "The Warp drive: Hyperfast travel within general relativity," Class. Quant. Grav. **11**, L73 (1994) doi:10.1088/0264-9381/11/5/001 [gr-qc/0009013].

[6] Davis, E. W. , (2009) "Chapter 15: Faster-Than-Light Approaches in General Relativity," Frontiers of Propulsion Science, Progress in Astronautics & Aeronautics Series, Vol 227, American Inst. of Aeronautics & Astronautics Press, Reston, VA, (2nd printing with corrections, 2012), pp. 473 − 509.

[7] S. V. Krasnikov, (1998) "Hyperfast travel in general relativity," Phys. Rev. D **57**, 4760 doi:10.1103/PhysRevD.57.4760 [gr-qc/9511068].

[8] Van Den Broeck, C. "A 'Warp drive' with reasonable total energy requirements," Class. Quant. Grav. **16**, 3973 (1999) doi:10.1088/0264-9381/16/12/314 [gr-qc/9905084].

[9] M. S. Morris and K. S. Thorne, (1988) "Wormholes in space-time and their use for interstellar travel: A tool for teaching general relativity," Am. J. Phys. **56**, 395. doi:10.1119/1.15620

[10] Morris, M. S., Thorne, K. S. and Yurtsever, U. (1988), "Wormholes, time machines, and the weak energy conditions," *Phys. Rev. Lett.*, Vol. 61, pp. 1446 − 1449.

[11] Visser, M. (1995), *Lorentzian Wormholes: From Einstein to Hawking* (New York: AIP Press).

[12] F. S. N. Lobo (2017), "Wormhole Basics," in *Wormholes, Warp Drives and Energy Conditions*, Fund. Theor. Phys. **189**, ed. F. S. N. Lobo, Springer, Cham, CH, pp. 11-33. doi:10.1007/978-3-319-55182-1

[13] Christoffel, E. B. (1869), "Ueber die Transformation der homogenen Differentialausdrücke zweiten Grades," *Journal für die reine und angewandte Mathematik*, Vol. 70, pp. 46 − 70.

[14] Zakhary, E. and McIntosh, C. B. G. (1997), "A Complete Set of Riemann Invariants," *Gen. Relativ. Gravit.*, Vol. 29, pp. 539 − 581.

[15] Carminati, J. and McLenaghan, R. G. 1991 "Algebraic invariants of the Riemann tensor in a four-dimensional Lorentzian space" *Journal of Mathematical Physics*, Vol. 32, Num. 11, pp. 3135 − 3140, doi:10.1063/1.529470.

[16] K. Santosuosso, D. Pollney, N. Pelavas, P. Musgrave and K. Lake, "Invariants of the Riemann tensor for class B warped product spacetimes," *Comput. Phys. Commun.* **115**, 381 (1998) doi:10.1016/S0010-4655(98)00134-9 [gr-qc/9809012].

[17] Henry, R. C. (2000), "Kretshmann Scalar for a Kerr-Newman Black Hole," *The Astrophysical Journal*, Vol. 535, pp. 350 – 353.

[18] J. G. Baker and M. Campanelli, "Making use of geometrical invariants in black hole collisions," Phys. Rev. D **62**, 127501 (2000) doi:10.1103/PhysRevD.62.127501 [arXiv:gr-qc/0003031 [gr-qc]].

[19] M. Abdelqader and K. Lake, "Invariant characterization of the Kerr spacetime: Locating the horizon and measuring the mass and spin of rotating black holes using curvature invariants," Phys. Rev. D **91**, no.8, 084017 (2015) doi:10.1103/PhysRevD.91.084017 [arXiv:1412.8757 [gr-qc]].

[20] MacCallum, M. A. H. (2015), "Spacetime invariants and their uses," arXiv:1504.06857v1 [gr-qc].

[21] D. Brooks, M. A. H. MacCallum, D. Gregoris, A. Forget, A. A. Coley, P. C. Chavy-Waddy and D. D. McNutt, (2018) "Cartan Invariants and Event Horizon Detection, Extended Version," Gen. Rel. Grav. **50**, no. 4, 37 [arXiv:1709.03362 [gr-qc]].

[22] H. Stephani, D. Kramer, M. A. H. MacCallum, C. Hoenselaers and E. Herlt, "Exact solutions of Einstein's field equations," doi:10.1017/CBO9780511535185

[23] R. L. Arnowitt, S. Deser and C. W. Misner, (1959)"Dynamical Structure and Definition of Energy in General Relativity," Phys. Rev. **116**, 1322 . doi:10.1103/PhysRev.116.1322

[24] P. Marquet, "The Generalized Warp Drive Concept in the EGR Theory."(2009) The Abraham Zelmanov Journal. No. 2.

[25] Bronnikov, K. A. (1973), "Scalar-tensor theory and scalar charge," *Acta Physica Polonica*, Vol. B4, pp. 251 – 266.

[26] C. Barcelo and M. Visser, "Twilight for the energy conditions?," Int. J. Mod. Phys. D **11**, 1553 (2002) doi:10.1142/S0218271802002888 [gr-qc/0205066].

[27] R. C. Woods, R. M. L. Baker, F. Li, G. V. Stephenson, E. W. Davis, and A. W. Beckwith, (2011) "A new theoretical technique for the measurement of high-frequency relic gravitational waves." Journal of Modern Physics **2**, pp. 498 – 518 doi:10.4236/jmp.2011.26060